



1           **Variations of surface roughness on inhomogeneous underlying**  
2           **surface at Nagqu Area over the Tibetan Plateau**

3           Maoshan Li<sup>\*1</sup>, Lei Shu<sup>1</sup>, Xiaoran Liu<sup>1</sup>, Shucheng Yin<sup>1</sup>, Lingzhi Wang<sup>1</sup>, Wei Fu<sup>1</sup>,  
4           Yaoming Ma<sup>2</sup>, Fanglin Sun<sup>3</sup>

5           (1.School of Atmospheric Sciences/Plateau Atmosphere and Environment Key Laboratory of Sichuan  
6           Province/Joint Laboratory of Climate and Environment Change, Chengdu University of Information Technology,  
7           Chengdu 610225, Sichuan China;

8           2. Key Laboratory of Tibetan Environment Changes and Land Surface Processes, Institute of Tibetan Plateau  
9           Research, Chinese Academy of Sciences, CAS Center for Excellence in Tibetan Plateau Earth Sciences, Beijing,  
10           China;

11           3. Key Laboratory of Land Surface Process and Climate Change in Cold and Arid Regions, Chinese Academy  
12           of Sciences. Lanzhou, China)

13  
14   **Abstract:** Using the MODIS satellite data and station atmospheric turbulence observation data in  
15   Nagqu area of northern Tibetan plateau in 2008, 2010 and 2012, with the Massman retrieved  
16   model and an independent method to determine aerodynamic surface roughness, the temporal and  
17   spatial variation characteristics of the surface roughness was analyzed. The results show that the  
18   surface roughness has obvious seasonal variation characteristics. From February to August, Z0m  
19   increases constantly with the ablation of snow and vegetation growth, and the maximum value  
20   reaches 4-5cm at BJ site. From September to February, Z0m gradually decreased because of the  
21   post-monsoon over the plateau, and the values decreased to about 1-2cm. The snowfall in  
22   abnormal years is the main reason why Z0m is obviously lower than that in normal. The  
23   underlying surface can be divided into four categories according to the different values of Z0m:  
24   snow and ice, sparse grassland, lush grassland and town. Among them, lush grassland and sparse  
25   grassland account for 62.49% and 33.74% respectively in the region, which are the main

---

\* Corresponding author

Dr. Maoshan Li

Chengdu University of Information Technology

24 Block 1, Xuefu Road, Chengdu 610225, Sichuan, China

E-mail: lims@cuit.edu.cn



26 categories, and their Z0m annual changes are between 2-6cm and 1-4cm. The correlation between  
27 the two methods are positively related to each other, and the retrieved data are smaller than the  
28 measured results due to the average sliding action. On the whole, Z0m calculated by satellite data  
29 retrieved algorithm is feasible, it can be applied to improve the model parameters of land surface  
30 model parameters and the accuracy of model simulation, better reveal the heat flux exchange.

31 **Key words:** Northern Tibet Plateau; Surface roughness; NDVI; MODIS

32

## 33 **1 Introduction**

34 Known as the "third pole" of the earth (Jane, 2008), the Tibetan plateau has an average  
35 altitude of over 4000m, accounting for a quarter of China's territory. It is located in the southwest  
36 of China, adjacent to the subtropical tropics in the south and reaching the mid-latitude in the north,  
37 making it the highest plateau in the world. Due to its special geographical location and  
38 geomorphic characteristics, it plays an important role in the formation, outbreak, duration and  
39 intensity of Asian monsoon especially in the global climate system. (Yang et al., 1998; Zhang et  
40 al., 1998; Wu et al., 1999, 2004, 2005; Ye et al, 1998; Wu et al, 1998; Tao et al, 1998). Lots of  
41 research shows that (Wu et al., 2013; Wang, 1999; Ma et al, 2002) the land-atmosphere interaction  
42 on the Tibet plateau plays an important role in regional and global climate. Wang (Wang, 1999)  
43 pointed out that high latitude areas and mountainous areas are sensitive areas of climate change,  
44 especially the land-atmosphere interaction located in the plateau area of middle latitude (including  
45 large areas of permafrost), which plays an extremely important role in regional climate and global  
46 climate. The plateau monsoon is closely related to the intensity and location of the south Asian  
47 high (Xun et al, 2002). The correlation between the dynamic index of plateau monsoon and the  
48 pelagic meridional wind shows that there is a teleconnection in summer, indicating that the  
49 teleconnection is the relationship between the plateau monsoon, the East Asian monsoon and the  
50 South Asian monsoon. In the past 47 years, the Tibetan plateau has shown a significant warming  
51 trend and increased precipitation. (Li et al., 2010) The thermal effects of the Tibetan Plateau not  
52 only have an important impact on the Asian monsoon and precipitation variability, but also affect  
53 the atmospheric circulation and climate in North America and Europe and the South Indian Ocean



54 by inspiring large-scale teleconnections similar to the Asia-Pacific Oscillation. (Zhou et al., 2009).

55 The various thermal and dynamic effects of the Tibetan Plateau on the atmosphere affect the  
56 free atmosphere through the atmospheric boundary layer. Therefore, it is particularly important to  
57 analyze the micro-meteorological characteristics of the atmospheric boundary layer of the  
58 Qinghai-Tibet Plateau, especially the near-surface layer. (Li et al., 2000). Affected by the unique  
59 underlying surface conditions of the Tibetan Plateau, local heating shows interannual and  
60 interdecadal variability (Zhou et al., 2009). Land-atmosphere interaction refers to a series of  
61 complex processes such as thermodynamics, dynamic, hydrology, biophysical and biochemical  
62 processes that occur on land surface, and the interaction process between these processes and the  
63 atmosphere (Su et al., 1999). Different underlying surfaces have different diversity, complex  
64 composition and uneven distribution. They also make the land surface composed of them diverse  
65 and complex. As the main input of atmospheric energy, the surface greatly affects the various  
66 interactions between the ground and the atmosphere, and even plays a key role in local areas or  
67 specific time (Guan et al, 2009). For this reason, the study of the land-atmosphere interaction on  
68 the Tibetan Plateau has become one of the research hotspots in the past 30 years, and has received  
69 more and more attention on the whole world.

70 The climate system is sensitive to anomalous changes in land surface conditions. The surface  
71 characteristic parameters (dynamic roughness, thermodynamic roughness, etc.) play an important  
72 role in the land surface process and are important factors in causing climate change (Jia et al.,  
73 2000). There are different degrees of fluctuant on the underlying surface of the Tibetan Plateau,  
74 which brings certain obstacles to understanding the land-atmosphere interaction of the Tibetan  
75 Plateau. The fluctuant surface may alter the arrangement of roughness element which on the  
76 surface and cause changes in surface roughness. Changes in roughness can also affect changes in  
77 the characteristics of other surface turbulent transportation, which may also result in changes in  
78 surface fluxes. Chen et al., (2015) presents a practical approach for determining the aerodynamic  
79 roughness length at fine temporal and spatial resolution over the landscape by combining remote  
80 sensing and ground measurements. And the surface roughness is an important parameter in the  
81 land surface model and climate model. Its size reflects the matter energy exchange, transmission



82 intensity and interaction between the near surface airflow and the underlying surface to some  
83 extent. (Liu et al., 2007; Irannejad et al, 1998; Shao et al, 2000; Zhang et al., 2003). Zhou et al.  
84 (2012) demonstrated that simulated sensible heat flux compared with measurement was  
85 significantly improved by using a time-dependent  $z_0$ . Therefore, the primary objective of this  
86 study is to calculate the surface roughness and its variation characteristics so that furthermore  
87 understanding of land-atmosphere interactions on the central of the Tibetan Plateau.

88 The Nagqu area is located in the hinterland of the Tibetan Plateau and is located in the the  
89 central of the Tibetan Plateau. It is the source of the Yangtze River, the Nujiang River, the Lhasa  
90 River and the Yigong River. The whole terrain is inclined to the west and the east is low, with an  
91 average elevation of over 4,500 meters. The altitude is high, the heat is insufficient, the climate is  
92 cold and dry, and the oxygen content is only half of the sea level. The Tibetan Plateau is one of the  
93 worst climatic conditions in Tibet. It is a typical sub-cold climate zone. Alpine and hypoxia, dry  
94 climate, large temperature difference between day and night, windy weather. (Li et al., 2004)  
95 However, there is a vast natural grassland here, so a complete mesoscale observation network  
96 centered on the Nagqu climate observation and research station has been established, and a large  
97 amount of valuable observation data has been obtained for more accurate description to provide  
98 sufficient evidence for Plateau land-atmosphere interactions and atmospheric boundary layer  
99 structures. The underlying surface of the Nagqu area is a vast highland plain, and the vegetation is  
100 alpine grassland. However, the underlying surface has different degrees of ups and downs and has  
101 certain complexity, which brings certain difficulties for the meticulous profound study of the  
102 land-atmosphere interaction on the Tibetan Plateau.

103 In this study, the satellite data is obtained by MODIS, and the normalized difference  
104 vegetation Index (NDVI) is studied through the Nagqu area to obtain the dynamic surface  
105 roughness. And using three observation stations in the region, atmospheric turbulence observation  
106 data from 2008, 2010, and 2012 and observation data from automatic weather stations, an  
107 independent method for determining surface dynamics roughness  $Z_0$  is applied (Chen et al.,  
108 1993). Analyzed time-scale dynamics of  $Z_0$  and the different results of different underlying  
109 surfaces. Through a comparative research on studying whether the value of surface roughness is



110 reliable, in order to provide accurate surface characteristic parameters for the study of  
111 land-atmosphere interaction in the plateau region, and to improve the theoretical research level of  
112 the near-surface layer in the Tibetan Plateau. In the following section, we describe the case study  
113 area, the MODIS remote sensing data, the ground observations, and the land cover map used to  
114 drive the revised Massman model (Massman et al, 1997, 1999). In Section 3, we present the  
115 results, followed by a validation based on flux measurements on Nagqu station. Finally, we give  
116 some concluding remarks on variation characteristics of the aerodynamic roughness lengths on the  
117 Nagqu area in the central of the Tibetan Plateau.

118

## 119 **2 Study area, Data and methods**

### 120 **2.1 Study area and Data**

121 The area selected in this study is a 200×200km<sup>2</sup> area centered on the Nagqu Station of  
122 Plateau Climate and Environment of the Northwest Institute of Ecology and Environmental  
123 Resources, Chinese Academy of Sciences, Northern Tibet Plateau.

124 In this area, there are North Pam (Portable Automated Meso-net) Automatic Meteorological  
125 Observatory (NPAM), Nam Co Station for Multisphere Observation and Research, Chinese  
126 Academy of Sciences (NAMC), and BJ three meteorological observatories stations (Figure 1).The  
127 underlying surface around the observation point is relatively flat on a small spatial scale, and there  
128 is a certain undulation at a large spatial scale. The data used included atmospheric turbulence  
129 observations and observations from automatic meteorological stations.

130 The BJ station is located at 31.37°N, 91.90°E, and the altitude is 4509m a.s.l. The BJ  
131 observation point is located in the seasonal frozen soil area, and the vegetation is alpine grassland.  
132 The site measurement equipment includes ultrasonic anemometer (CAST3), CO<sub>2</sub>/H<sub>2</sub>O infrared  
133 open circuit analyzer (LI 7500) and automatic meteorological observation system. (Ma et al., 2006)  
134 This study uses the data of BJ station in 2008 and 2012. The NPAM station is located at 31°56'N,  
135 91°43'E and has an altitude of approximately 4700m. The ground of the experimental field is flat  
136 and the area is wide. The ground is covered by a plateau meadow 15 cm high in summer. The  
137 experimental station observation equipment includes ultrasonic wind thermometer and humidity



138 probepulsator, and also includes data on temperature and humidity, air pressure, average wind  
139 speed, average wind direction, surface radiation temperature, soil heat flux, soil moisture and  
140 temperature, and radiation. (Ma et al., 2006) This thesis uses the NPAM station's 2012 full year  
141 data. The NAMC station is located at 30°46.44'N, 90°59.31'E, at an altitude of 4730m. It is  
142 located on the southeastern shore of Namco Lake in Namuqin Township, Dangxiong County, Tibet  
143 Autonomous Region. It is backed by the Nyainqentanglha Mountain Range and the underlying  
144 surface is an alpine meadow. It is a typical semiarid plateau monsoon climate zone. The NAMCO  
145 station's 2010 full year data has been used in this study.

146 **Figure 1 about here**

147 **Table 1 about here**

148 The land cover data used in this study is GLC2009 (Arino et al, 2010) data. The data is the  
149 retrieved data of Envisat satellite in 2009 with a spatial resolution of 300m and the classification  
150 standard is Land Cover Classification System (LCCS). The classification standard divides the  
151 global surface into 23 different types, this thesis including the selected areas about 14 kinds. As  
152 the actual situation in the selected area does not match the data part of GLC2009, there is no  
153 underlying surface such as farmland in the selected area. Therefore, according to the actual land  
154 cover types obtained by Chu (Chu, 2010), the names of irrigated farmland, dry farmland, mixed  
155 farmland vegetation, mixed multi-vegetation land, closed grassland and open grassland are  
156 replaced with 6 grassland, shrub meadows, mountain meadows, alpine grasslands, alpine  
157 meadows and sparse vegetation in the mountains. Since the proportion of the underlying surface  
158 of the tree as a whole is only 0.36%, the four types of underlying surfaces of the evergreen  
159 coniferous forest, the mixed forest, the multi-forest grassland mix and the multi-grass forest land  
160 mix will no longer be studied.

161 The satellite data from the MODerate-resolution Imaging Spectroradiometer (MODIS) is an  
162 important sensor in the satellites TERRA and AQUA launched by the US Earth Observing System  
163 Program. The band of MODIS sensor covers the full spectrum of visible light to thermal infrared,  
164 which can detect surface and atmospheric conditions such as surface temperature, surface  
165 vegetation cover, atmospheric precipitation, cloud top temperature, etc. The maximum spatial



166 resolution is 250m. The normalized vegetation index obtained by MODIS detection is the  
 167 MYD13Q1 product from MODIS, which provides a global resolution of 250m per 16 days. This  
 168 study selects 73 materials for the year of 2008, 2010 and 2012 in Nagqu.

## 169 2.2 Methodology

### 170 2.2.1 Method for calculating surface roughness by observation data

171 Using the measured values of average wind speed and turbulent flux of a single height  
 172 ultrasonic anemometer, the calculation scheme of surface roughness proposed by Chen et al.  
 173 (Chen et al., 1993) was selected and the dynamic variation of the surface roughness was obtained.

174 According to the Monin-Obukhov similarity theory (Monin et al., 1954), the wind profile  
 175 formula with the stratification stability correction function (Panosky et al, 1984) is

$$176 \quad U(z) = \frac{u_*}{k} \left[ \ln \frac{z-d}{Z_{0m}} - \psi_m(\zeta) \right] \quad (2.1)$$

$$177 \quad \psi_m(\zeta) = 2 \ln \left( \frac{1+x}{2} \right) + \ln \left( \frac{1+x^2}{2} \right) - \tan^{-1}(x) + \frac{\pi}{2} \quad \zeta < 0 \quad (2.2)$$

$$178 \quad \psi_m(\zeta) = -5\zeta \quad \zeta > 0 \quad (2.3)$$

179 Where:  $Z_{0m}$  is the dynamic surface roughness length;  $z$  is the observed height;  $d$  is zero  
 180 plane displacement, taken as 0.03m (Yang et al., 2014), calculated from the average vegetation  
 181 height 0.045m;  $U$  is the average wind speed;  $k$  is the Karman constant, taken as 0.35;

$$182 \quad L = - \frac{u_*^3}{\left(k \frac{g}{\theta}\right) \theta' \omega'} \quad (\text{Monin et al., 1954 is the Monin-Obukhov length; } x = (1 - 16\zeta)^{1/4};$$

183  $\zeta = (z-d)/L$  is the atmospheric stability parameter. Available from formula (2.1):

184

$$185 \quad \ln \frac{z-d}{Z_{0m}} = \frac{kU}{u_*} + \psi_m(\zeta) \quad (2.4)$$

186 Using equations (2.2)-(2.4),  $Z_{0m}$  can be determined by fitting  $\zeta$  and observation of a single

187 height  $\frac{kU}{u_*}$ .



188 **2.2.2 Method for calculating surface roughness by satellite data**

189 For fully covered uniform canopy, Brutsaert suggest that  $z_{0m} = 0.13h_v$  (Brutsaert, 1982). For  
190 the canopy with proportional coverage (partial coverage), according to the research of Raupach  
191 (Raupach, 1994),  $z_{0m}/h_v$  varies with the leaf area index  $I$ . However, Pierce et al. (Pierce et al.  
192 1992) pointed out that for all kinds of biological groups, leaf area index can be obtained from  
193 NDVI, and the density grade of vegetation can be related to NDVI. Asrar et al (Asrar et al., 1992)  
194 pointed out that there was mutual relationship between LAI, NDVI and ground cover through the  
195 study of physical model. Moran's study (Moran, et al., 1994) gives another way, using a function  
196 of the relationship between NDVI and  $Z_{0m}$  in the growing season of alfalfa,

197 
$$Z_{0m}(x, y) = \exp [C_1 + C_2 NDVI(x, y)] \quad (2.5)$$

198 Where  $C_1$  and  $C_2$  are empirical constants.

199 Considering that the main underlying surface of the study area is grassland, this study selects  
200 the Massman model (Massman et al, 1997, 1999) to calculate the  $Z_{0m}$  in Nagqu area of central of  
201 the Tibetan Plateau. The Massman model is calculated as follows:

202 
$$\gamma = C_1 + C_2 \cdot \exp(-C_3 \cdot C_d \cdot LAI) \quad (2.6)$$

203 
$$n_{ec} = \frac{C_d \cdot LAI}{2 \cdot \gamma^2} \quad (2.7)$$

204 
$$d_h = 1 - \frac{[1 - \exp(-2 \cdot n_{ec})]}{2 \cdot n_{ec}} \quad (2.8)$$

205 
$$\frac{Z_{0m}}{h} = [1 - d_h] \cdot \exp\left(-\frac{k}{\gamma}\right) \quad (2.9)$$

206 Among them,  $C_1=0.32$ ,  $C_2=0.26$ ,  $C_3=15.1$  is the constant in the model, which is related to  
207 the surface drag coefficient, LAI is the leaf area index,  $C_d=0.2$  is the liquid surface drag  
208 coefficient,  $n_{ec}$  is the wind speed profile coefficient of fluctuation in the vegetation canopy,  $h$  is the  
209 vegetation height. In many earlier studies, it was concluded that the high-altitude environment of  
210 the Tibetan Plateau caused a low temperature in the area to which the study was located, and had  
211 an effect on the height and sparseness of the vegetation. Based on the previous researches, this  
212 study considers that the vegetation height in northern Tibet is related to the normalized differential





213 vegetation index (NDVI) and altitude (Chen et al, 2013), and introduced the altitude correction  
214 factor on the original basis. The following is the calculation formula.

$$215 \quad H = h_{\min} + \left( \frac{h_{\max} - h_{\min}}{NDVI_{\max} - NDVI_{\min}} \right) (NDVI - NDVI_{\min}) \quad (2.10)$$

$$216 \quad h = acf \cdot H \quad (2.11)$$

217 Among them,  $h_{\min}$  and  $h_{\max}$  are the minimum and maximum values of vegetation height  
218 observed at the observation station, and  $NDVI_{\max}$  and  $NDVI_{\min}$  are the maximum and minimum  
219 values of NDVI of the observation station.  $H$  is based on the assumption that the vegetation height  
220 is directly proportional to the NDVI.  $x$  is the altitude and is obtained from ASTER's DEM  
221 products.  $acf$  is the altitude correction factor (Sun et al., 2016), which is used to characterize the  
222 effect of altitude elevation on the height of vegetation in northern Tibet. Its form is:

$$223 \quad acf = \begin{cases} 0.149, & x > 4800 \\ 11.809 - 0.0024 \cdot x, & 4300 < x < 4800 \\ 1.49, & x < 4300 \end{cases} \quad (2.12)$$

224 The LAI used in this thesis is calculated by the NDVI of MODIS. The calculation formula is:

$$225 \quad LAI = \left( \frac{NDVI * (1 + NDVI)}{1 - NDVI} \right)^{0.5} \quad (2.13)$$

## 226 **3 Result analysis**

### 227 **3.1 The variation characteristics of surface roughness by using measured data**

228 Figure 2 shows the temporal variation characteristics of surface roughness of sites in different  
229 years in Nagqu area. It can be seen that  $Z0m$  value has continued to increase since February to  
230 reach a maximum in July and August. The BJ station and the NPAM station in 2012 show that  
231 July is slightly larger than that in August, the 2010 NAMCO station and the 2008 BJ station in  
232 August is bigger than July. The BJ station may have a precipitation process in July 2008, resulting  
233 in a July  $Z0m$  value less than June. After August,  $Z0m$  began to decrease, and the value of  
234 December was about the same as the value of January. In general, the change of  $Z0m$  degree of  
235 each station increases from spring to summer and decreases month by month from summer to  
236 winter.



237 **Figure 2 about here**

238

239 **3.2 Spatiotemporal variation characteristics of surface roughness length**  
240 **retrieved of MODIS data**

241 Figure 3 is a plot of surface roughness distribution of  $200 \times 200 \text{ km}^2$  around the BJ site in  
242 2008. In February, the  $Z0m$  decreased from January, which may be due to snowfall, temperature,  
243 etc., resulting in a small  $Z0m$  and continued to decrease. Due to the rising temperature of snow  
244 melting,  $Z0m$  showed a slowly increasing trend from February to May, and  $Z0m$  showed a rapid  
245 increase from June to August. From June onwards, a large number of surface textures are presented,  
246 indicating the complexity of the underlying surface. Whether it is the bulk surface or the  
247 vegetation, it will have an important impact on  $Z0m$ . From May to August, due to the obvious  
248 changes in humidity, temperature and pressure caused by the plateau summer monsoon, the height  
249 and coverage of surface vegetation increased, and  $Z0m$  peaked in August. In particular, the change  
250 from May to June is very significant. It may be due to the beginning of the summer monsoon in  
251 June, which led to the increase of precipitation, which accelerated the growth of vegetation and  
252 the rapid rise of  $Z0m$ . In June, July and August, due to continuous precipitation and rising  
253 temperature, the vegetation growth flourishes, but it does not change after the growth to maturity.  
254 Corresponding to the maximum value of  $Z0m$  in the figure, but due to sufficient moisture,  $Z0m$   
255 gradually expanded during the three months, reaching the maximum range in August in the large  
256 area. From September to December, as the plateau summer monsoon subsides, the temperature  
257 and humidity are gradually reduced. Compared with the plateau summer monsoon, the vegetation  
258 is no longer suitable for vegetation growth, the contribution of vegetation to  $Z0m$  is weakened,  
259 and the surface vegetation height is the coverage gradually decreases, and thus,  $Z0m$  continues to  
260 decrease, and the range of large-value regions also gradually decreases.

261 **Figure 3 about here**

262 **Figure 4 about here**

263 Figures 4 and 5 respectively show the retrieved monthly surface roughness in the BJ area  
264 in 2010 and 2012. It can also be seen that the  $Z0m$  also showed a decrease from January to  
265 February in the Nagqu area in 2010 and 2012. Since February,  $Z0m$  has started to increase. Since



266 June, Z0m has grown rapidly and reached the peak of the whole year in August. After that, Z0m  
267 began to decrease.

268 **Figure 5 about here**

269 It can also be seen from Fig. 3, Fig. 4, Fig. 5 that Z0m changes with spatial and temporal  
270 scale. Z0m shows different trends on different underlying surfaces. It is worth noting that in  
271 November 2008, the Z0m in the Nagqu area was small overall, generally as low as 1 cm.  
272 According to historical data, it is known that there is a large-scale snowfall process in the Naqu  
273 area at this time. The snowfall of the meadow causes the underlying surface of the meadow to be  
274 homogeneous and flat, and after the snowfall falls, it is easy to form a block, scattered and  
275 discontinuous underlying surface. And it can be obtained later that the surface roughness of the  
276 area with ice and snow as the underlying surface is not more than 1 cm, which is consistent with  
277 the historical weather process. So think that snowfall caused the Z0m in November to be very  
278 small. And from November to December, Z0m showed a growing trend, which may be due to  
279 temperature, soil unfrozen or other reasons, resulting in the melting of snow, and then the surface  
280 roughness showed a growing trend (Zhou, 2017).

281 3.3 Evaluation of satellite data retrieved results

282 **Figure 6 about here**

283 The underlying surfaces of the three sites selected in this thesis are all alpine meadows. In  
284 Figure 6, the NPAM site data calculation results are larger than the satellite data retrieved results  
285 throughout the year, only September and October are very close, and the trend is similar. The  
286 maximum value of the site data calculation is 5cm and the satellite data retrieved result is 4.5cm  
287 maximum. The maximum difference is in May, which is 1.7cm. The NAMCO station data  
288 calculation results are very close to the satellite data retrieved results from April to November, but  
289 the satellite data retrieved results in January, March and December are significantly larger than the  
290 site data calculation results. The biggest difference appears in January, and the difference value is  
291 up to 1.5cm. In 2008, the calculation results of BJ station data were larger than the satellite data  
292 retrieved results throughout the year. The calculation results of the site data were very close to the  
293 satellite data retrieved results from January to April, July to November, but there was a big  
294 difference between the May June and December, and the biggest difference occurred in May, with  
295 a difference of 1.8 cm. In 2012, BJ's site data calculation results were consistent with the satellite



296 data retrieved results for the whole year, but the site data calculation results were larger than the  
297 satellite data retrieved results from March to June, and the station data calculation results were  
298 smaller than the satellite data retrieved at other times. As a result, the largest difference occurred  
299 in June with a difference of 1.1 cm. It can be seen from Figure 6 that, in the overall situation, in  
300 January, February, March, November and December, the seasonal variation trend of the site data  
301 calculation results is consistent with the satellite data retrieved results. However, the site data  
302 calculation results from April to October are greater than the satellite data retrieved results. From  
303 Fig. 6 the Z0m calculated from the site observation data is larger than the satellite data, which may  
304 be because the average smoothing effect. It is worth noting that from February to July, the single  
305 point Z0m value was significantly increased according to the independent method of determining  
306 the surface roughness, while the results obtained by using the satellite data did not increase  
307 significantly. The satellite results show that the January to May, November, and December are  
308 basically stable below 2cm, and only change from June to October; this is related to the  
309 overlapping averages effect of satellite data retrieved. In general, the results calculated by the  
310 station are generally larger than those obtained by satellite retrieved.

311 **Figure 7 about here**

312 The Z0m scatter plot is shown in Figure 7. It can be seen that there is a significant positive  
313 correlation between the satellite data and the surface roughness calculated from the site data. The  
314 correlation coefficient between the observation result and the retrieved result is different from that  
315 of the NAMCO station in 2010 in Fig. 7(g), and the others are large. It shows that the average  
316 result of the underlying surface smoothes the same underlying surface results in different regions,  
317 further indicating that the satellite retrieved results are more similar to the site calculation results.  
318 However, the results of the NAMCO site are different from those of other sites. The correlation  
319 coefficient with the results of the underlying surface is 0.83288, and the correlation coefficient  
320 with the satellite retrieved results is 0.61554. Or because the Namco Observation Station is closer  
321 to the lake (1km), it is more affected by local microclimate such as lake and land winds. The  
322 results in Figure 7 all passed the F test of  $P = 0.05$ . It indicates that there is no significant  
323 difference between the site data calculation results and the satellite data retrieved results.



324 **4 Variation characteristics of surface roughness of different**  
325 **underlying surfaces**

326 According to the vegetation data GLC2009 combined with local actual conditions, the  
327 200×200km<sup>2</sup> area of Nagqu was divided into 10 different underlying surfaces (Arino et al., 2010),  
328 namely: mountain grassland, shrub meadow, mountain meadow, alpine Grasslands, alpine  
329 meadows, sparse vegetation lap, urban land, bare land, water bodies, ice sheets and snow covers.

330  
331

**Figure 8 about here**

332 The monthly variation of Z0m in different underlying surfaces in Nagqu area is shown in Fig.  
333 8. According to the figure, 14 different underlying surfaces in the Nagqu area can be divided into  
334 four categories. The first category is urban land, accounting for 0.07% of the whole study area. All  
335 the time of the year is greater than the Z0m of other underlying surfaces, and the change of Z0m is  
336 very large, probably due to the irregular changes in the underground areas of the selected areas  
337 and the irregularities caused by human activities. The second category is lush grassland, including  
338 shrub meadows, mountain grasslands, alpine grasslands and mountain meadows, which account  
339 for 62.49% of the area. The variation curves of the four underlying surfaces Z0m are similar, and  
340 are only smaller than the urban land compared with other underlying surfaces. The third category  
341 is sparse grassland, including alpine sparse vegetation, alpine meadows and bare land, accounting  
342 for 33.74% of the area. The Z0m of the three underlying surfaces are similar, at a medium height.  
343 The Z0m of the bare soil is at the lowest point of these underlying surface Z0m, and the Z0m of  
344 the alpine meadow is relatively stable and less affected by the outside. The fourth category is ice  
345 and snow, including ice sheets and snow cover, water bodies two kinds of underlying surfaces,  
346 accounting for 3.7% of the area. The Z0m of these three underlying surfaces presents another  
347 phenomenon. The variation range of the whole year is relatively small, and the Z0m of these  
348 underlying surfaces is also small. It is more than 1cm in mid-June, and other times Z0m is less  
349 than 1cm. Figure 8(d) shows the multi-year average seasonal variation of Z0m. It can be clearly  
350 seen from the figure that the underlying surface can be divided into four categories due to the  
351 difference in surface roughness. And the change from January to May Z0m is very small, peaking  
352 from May to August, and then down to the previous January to May level in November and



353 December. Due to the snowfall in November 2008, it may lead to the low level of November in  
354 Figure 8(d). In fact, the surface roughness on November should be higher than that on December  
355 in former years.

356 It can also be seen from Fig. 8 that in the Nagqu area, except for the area of the fourth type of  
357 underlying surface, the Z0m change in other areas decreases from January to February, and begins  
358 to increase after February, reaching the peak on August, then starting to decrease. However, it can  
359 be clearly seen from Fig. 6 that there are several stages in which Z0m changes significantly, in  
360 early April, mid-May, early July, late August, and late September. The change at the end of August  
361 was the most obvious. Each of the underlying surfaces Z0m changes by more than 2 cm on  
362 average. The extent of the change in late September was also large, with an average change of  
363 more than 1.5 cm. It should also be pointed out that the change in early July was special because  
364 the change resulted in a significant increase in the Z0m of water bodies and ice.

365 It is worth noting that due to factors such as cloud cover, May, August, and November of  
366 2008; August and September of 2010; April and July of 2012, the overall Z0m has changed  
367 significantly. This resulted in two very significant changes in August and November on the  
368 three-year average. In November, according to other meteorological data, it was caused by  
369 snowfall. The reason for the August change caused by 2008 and 2010, through analyzing to the  
370 Z0m of the water body and the ice and snow surface suddenly increased, was caused by  
371 precipitation. Combined with several changes in Z0m, it can be analyzed that precipitation,  
372 snowfall, and snow accumulation will make the underlying surface more uniform and flat, and the  
373 Z0m will also be relatively reduced.

## 374 **5 Conclusion and discussion**

375 Through the calculation and analysis of the surface roughness of the Nagqu area in the  
376 central of the Tibetan Plateau, and comparing the retrieved of the satellite data with the calculation  
377 results of the observational data, the attained main conclusions are as follows:

378 (1) The retrieved results of the satellite data are basically consistent with the calculated  
379 results of the measured data. Both indicate that the surface roughness has continued to increase  
380 from February to August, and began to decrease after reaching the peak in August, and reached the



381 lowest value in February of the following year. There is a lot of connection between the monthly  
382 variation of surface roughness and the changes of meteorological elements brought by the plateau  
383 summer monsoon. Among them, the satellite surface retrieved results in a slow increase in surface  
384 roughness from February to May.

385 (2) Through the characteristics of surface roughness variation retrieved by satellite data, the  
386 underlying surface can be divided into four categories according to the surface roughness, from  
387 large to small, urban, lush grassland, sparse grassland and ice and snow. Among them, lush  
388 grassland accounts for 62.49%,  $Z_{0m}$  can reach 6cm, sparse grassland accounts for 33.74%,  $Z_{0m}$  can  
389 reach up to 4cm, ice and snow account for 3.7%, and  $Z_{0m}$  does not exceed 1cm.

390 (3) Comparing the results of satellite retrieved calculation, satellite retrieved results and  
391 measured data, the results are positively correlated, and the satellite retrieved results is better  
392 fitting with the measured results. Due to the average sliding effect of the retrieved, the satellite  
393 retrieved data is smaller than the measured results. This method can be used to calculate the  
394 surface roughness results for a region and provide a true value for the model for simulation.

395 Through the study of surface roughness, it is beneficial to obtain the surface feature  
396 parameter values on the region, provide the ground truth value for the model input, improve the  
397 simulation level of the model in the Tibetan Plateau, and deepen the understanding of the  
398 land-atmosphere interaction process.

#### 399 **Acknowledgements:**

400 This work was financially supported by the Second Tibetan Plateau Scientific Expedition and  
401 Research (STEP) program (Grant No. 2019QZKK0103), the National Natural Science Foundation  
402 of China (Grant No. 41675106) and National key research and development program of China  
403 (2017YFC1505702)

#### 404 **References:**

405 Arino O, Ramos J, Kalogirou V, et al. "Glob Cover 2009" [R].Edinburgh, UK: Proceedings of the  
406 living planet Symposium, 2010.  
407 Asrar , G ., Myneni , R.B.and Chaudhury , B.J., 1992, Spatial heterogeneity in vegetation canopies  
408 and remote sensing of observed photosynthetically active radiation:a modeling study ,



- 409 Ren.Sens.Env ., 41, 85~ 103.
- 410 Brutsaert , W.A ., 1982, Evaporation into the Atmosphere , Dordrecht in Holland , D .Reidel  
411 Publishing Company,113 ~ 121.
- 412 Chen, J.Y., Wang, J.M., Mitsuaki, H., 1993. An independent method to determine the surface  
413 roughness length. Chin. J. Atmos. Sci. 1993, 17, 21–26.
- 414 Chen Q., L. Jia, R. Hutjes, M. Menenti, 2015, Estimation of Aerodynamic Roughness Length over  
415 Oasis in the Heihe River Basin by Utilizing Remote Sensing and Ground Data, Remote Sensing,  
416 2015, 7(4), 3690-3709; doi:10.3390/rs70403690.
- 417 Chen X., et al, 2013. An improvement of roughness height parameterization of the Surface Energy  
418 Balance System (SEBS) over the Tibetan Plateau[J]. Journal of Applied Meteorology and  
419 Climatology, 52(3): 607-622.
- 420 Guan X., Huang J., et al, 2009. Variability of soil moisture and its relationship with surface albedo  
421 and soil thermal parameters over the Loess Plateau[J]. Advances in Atmospheric Sciences, 26(4):  
422 692-700, doi: 10.1007/s00376-009-8198-0.
- 423 Irannejad P, Shao Y P, 1998. Description and validation of the atmosphere-land-surface interaction  
424 scheme(ALSIS)with HAPEX and Cabauw data[J]. Global Planet Change, 19(1): 87-114.
- 425 Jane Q, 2008. The third pole[J]. Nature, 454(24): 393-396.
- 426 Ma Y., Tsukamoto O, Wang J., et al, 2002. Analysis of aerodynamic and thermodynamic  
427 parameters on the grassy marshland surface of Tibetan Plateau[J]. Progress in Natural Science,  
428 12(1): 36-40.
- 429 Massman W., 1997. An analytical one-dimensional model of momentum transfer by vegetation of  
430 arbitrary structure[J]. Boundary-Layer Meteorology, 83(3): 407-421.
- 431 Massman W., 1999. An analytical one-dimensional second-order closure model of turbulence  
432 statistics and the Lagrangian time scale within and above plant canopies of arbitrary structure[J].  
433 Boundary-Layer Meteorology, 91(1): 81-107.
- 434 Monin A., Obukhov A., 1954. Basic laws of turbulent mixing in the atmosphere near the ground[J].  
435 Tr Akad Nauk SSSR Geofiz Inst, 24(15): 163-187.
- 436 Moran, M .S ., Clarke , T .H., Inone, Y.et al., 1994, Estimating crop water deficit using the relation





437 between surface-air temperature and spectral vegetation index, *Rem .Sens. of Env .*, 49 , 246 ~  
438 263.

439 Panosky H., Dutton J., 1984. *Atmospheric Turbulence: Models and Methods for Engineering*  
440 *Applications*[M]. New York: John Wiley, 1-399.

441 Pierce , L.L., Walker, J., Downling , T .I.et al., 1992, Ecological change in the Murry -Darling  
442 Basin-III :A simulation of regional hydrological changes , *Journal of Applied Ecology* , 30, 283~  
443 294.

444 Raupach, M .R., 1994, Simplified expressions for vegetation roughness leng h and zero-plane  
445 displacement as functions of canopy height and area index , *Boundary -Layer Meteor .*, 71, 211-  
446 216.

447 Shao Y., 2000. *Phstics and Modeling of Wind Erosion*[M]. London: Kluwer Academic Publishers,  
448 1-452.

449 Stull B R, 1991. *An Introduction to Boundary Layer Meteorology*[M]. Beijing: China  
450 Meteorological Press, 1-737.

451 Tao S., Chen, L., Xu X., et al, 1998. *Progresses of the Theoretical Study in the Second Tibetan*  
452 *Plateau Experiment of Atmospheric Sciences(PartI)*[M]. Beijing: China Meteorological Press,  
453 1-348.

454 Wu G., Zhang Y., 1998. Tibetan Plateau forcing and timing of the Mon-soon onset over south Asia  
455 and the south China sea[J]. *Monthly Weather Review*, 4(126): 913-927.

456 Xun X., Hu Z., Ma Y., 2012. The dynamic Plateau Mon-soon Index and its association with  
457 general circulation an omaliesming[J]. *Advances in Atmospheric Sciences*, 29(6): 1249-1263,  
458 DOI: 10.1007/s00376-012-1125-9.

459 Ye D., Wu G., 1998. The role of heat source of the Tibetan Plateau in the general circulation[J].  
460 *Meteorological and Atmospheric Physics*, 67(1): 181-198.

461 Chen J., Wang J., Yasushi M., 1993. An Independent, Method to Determine the Surface Roughness  
462 Length[J]. *Scientia Atmospherica Sinica*, 17(01): 21-26. (in Chinese with English abstract)

463 Chu D., Basabta S., Wang W., et al, 2010. Land Cover Mapping in the Tibet Plateau Using  
464 MODIS Imagery[J]. *Resources Science*, 32(11): 2152-2159. (in Chinese with English abstract)



- 465 Jia L., Wang J., Hu Z., 2000. The Characteristics of Roughness Length for Heat and Its Influence  
466 on Determination of Sensible Heat Flux in Arid Zone[J]. Plateau Meteorology, 19(04): 495-503.  
467 (in Chinese with English abstract)
- 468 Li F., Li S., Chen T., 2004. A Study on Development of the Tibetan North Grasslands Tourism  
469 Stockbreeding in Naqv Tibet[J]. Sichuan Caoyuan, 109(12): 38-42. (in Chinese with English  
470 abstract)
- 471 Li J., Hong Z., Sun S., 2000. An Observational Experiment on the Atmospheric Boundary Layer in  
472 Gerze Area of the Tibetan Plateau[J]. Chinese Journal of Atmospheric Sciences, 24(03): 301-312.  
473 (in Chinese with English abstract)
- 474 Li L., Chen X., Wang Z., et al, 2010. Climate Change and Its Regional Differences over the  
475 Tibetan Plateau[J]. Advances in Climate Change Research, 6(03): 181-186. (in Chinese with  
476 English abstract)
- 477 Liu J., Zhou M., Hu Y., 2007. Discussion on the Terrain Aerodynamic Roughness[J]. Ecology and  
478 Environment, 16(06): 1829-1836. (in Chinese with English abstract)
- 479 Ma Y., Wang J., et al, 2002. Analysis of Aerodynamic and Thermodynamic Parameters on the  
480 Grassy Marshland Surface of Tibetan Plateau[J]. Peogress in Natural Science, 12(01): 36-40. (in  
481 Chinese with English abstract)
- 482 Ma Y., Yao T., Wang J., et al, 2006. The Study on the Land Surface Heat Fluxes over  
483 Heterogeneous Landscape of the Tibetan Plateau[J]. Advances in Earth Science, 21(12):  
484 1215-1223. (in Chinese with English abstract)
- 485 Su B., Zhao M., Ren J., 1999. Influence of Scalar Roughness Lengths on the  
486 Biosphere-Atmosphere Transfer[J]. Chinese Journal of Atmospheric Sciences, 23(03): 349-358.  
487 (in Chinese with English abstract)
- 488 Sun G., 2016. The Upscaling Analysis of Surface Fluxes of Alpine Grassland over the in Northern  
489 Tibetan Plateau[D]. Lanzhou: Cold and Arid Regions Environmental and Engineering Research  
490 Institute Chinese Academy of Science, 1-134. (in Chinese with English abstract)
- 491 Wang J., 1999. Land Surface Process Experiments and Interaction Study in China-from HEIFE to  
492 Imgrass and GAME-TIBET/TIPEX[J]. Plateau Meteorology, 18(03): 280-294. (in Chinese with



- 493 English abstract)
- 494 Wu G., Liu Y., Liu X., et al. 2005. How the heating over the Tibetan Plateau affects the Asian  
495 climate in summer[J]. Chinese Journal of Atmospheric Sciences, 29(1): 47-56. (in Chinese with  
496 English abstract)
- 497 Wu G., Mao J., Duan, A., et al., 2004. Recent progress in the study on the impact of Tibetan  
498 Plateau on Asian summer climate[J]. Acta Meteorologica Sinica, 62(5): 528-540. (in Chinese  
499 with English abstract)
- 500 Wu G., Zhang Y., 1999. Thermal and Mechanical Forcing of the Tibetan Plateau and Asian  
501 Monsoon Onset.Part II :Timing of the Onset[J]. Chinese Journal of Atmospheric Sciences,  
502 23(01): 52-62. (in Chinese with English abstract)
- 503 Wu X., Ma W., Ma Y., 2013. Observation and Simulation Analyses on Characteristics of Land  
504 Surface Heat Flux in Noethern TibetanPlateau in Summer[J]. Plateau Meteorology, 32(05):  
505 1246-1252. (in Chinese with English abstract)
- 506 Yang M., Yao T., 1998. A Review of the Study on the Impact of Snow Cover in the Tibetan  
507 Plateau on Asian Monsoon[J]. Journal of Glaciology and Geocryolgy, 20(2): 90-95. (in Chinese  
508 with English abstract)
- 509 Yang Y., Li M., Hu Z., et al., 2014. Influence of surface roughness on surface-air fluxes in alpine  
510 meadow over the Norther TibetanPlateau[J].Plateau Meteor, 33(3): 626-636. (in Chinese with  
511 English abstract)
- 512 Zhang Q., Lv S., 2003. The Determination of Roughness Length over City Surface[J]. Plateau  
513 Meteorology, 22(01): 24-32. (in Chinese with English abstract)
- 514 Zhang Y., Wu G., 1998. Diasnostic Investigations of Mechanism of Onset of Asian Summer  
515 Monsoon and Abrupt Seasonal Transitions Over Northern Hemisphere PartI[J]. Acta  
516 Meteorologica Sinica, 56(5): 2-17. (in Chinese with English abstract)
- 517 Zhou X., Zhao P., Chen J., et al, 2009. Impacts of Thermodynamic Processes over the Tibetan  
518 Plateau on the Northern Hemispheric Climate[J]. Sci China Ser D-Earth Sci, 39(11): 1473-1486.  
519 (in Chinese with English abstract)
- 520 Zhou, Y., Ju, W., Sun, X., Wen, X., Guan, D. 2012 Significant decrease of uncertainties in sensible



521 heat flux simulation using temporally variable aerodynamic roughness in two typical forest  
522 ecosystems  
523 of China. *J. Appl. Meteorol. Climatol.* 2012, 51, 1099–1110.  
524 Zhou Y., Xu W., Bai A., et al, 2017. Dynamic Snow-melting Process and its Relationship with Air  
525 Temperature in Tuotuohe, TibetanPlateau[J]. *Plateau Meteorology*, 36(1): 24-32. (in Chinese  
526 with English abstract)  
527










- 528 Figure captions
- 529 Fig. 1 The location of sites and the land cover on the northern of the Tibetan Plateau. The black
- 530 solid circle '●' is location of the sites
- 531 Fig. 2 The surface roughness length of different site on the northern of the Tibetan Plateau
- 532 Fig. 3 The surface roughness length on the northern of the Tibetan Plateau in 2008
- 533 Fig. 4 The surface roughness length on the northern of the Tibetan Plateau in 2010
- 534 Fig. 5 The surface roughness length on the northern of the Tibetan Plateau in 2012
- 535 Fig. 6 Comparison of surface roughness length by site observation and satellite remote sense
- 536 retrieved
- 537 Fig. 7 Site surface roughness length scatter plot
- 538 Fig. 8 The curve of the surface roughness length in different underlying surface
- 539









540 Tables

541 Table. 1 The legend of the land cover map on the northern of the Tibetan Plateau

Value	Color	Land Cover Types	Percent (%)
11		Mountain grassland	5.79
14		Shrub meadow	3.25
20		Mountain meadow	8.26
30		Alpine grassland	45.16
70		Needleleaved evergreen forest	0.23
100		Mixed forest	0.03
110		Mixed forestland and grassland	0.06

542

Value	Color	Land Cover Types	Percent (%)
120		Mixed grassland and	0.04
140		Alpine meadow	28.28
150		Alpine sparse vegetation	0.29
190		Urban areas	0.07
200		Bare areas	4.90
210		Water bodies	2.57
220		Permanent Snow and ice	1.07

543

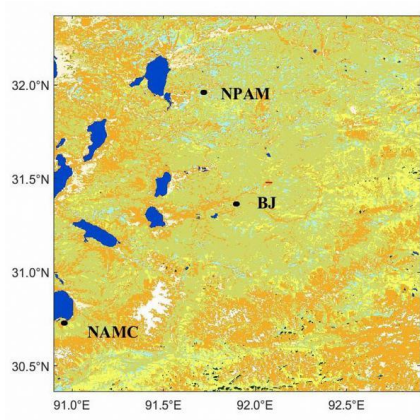
544

545

546

547

548

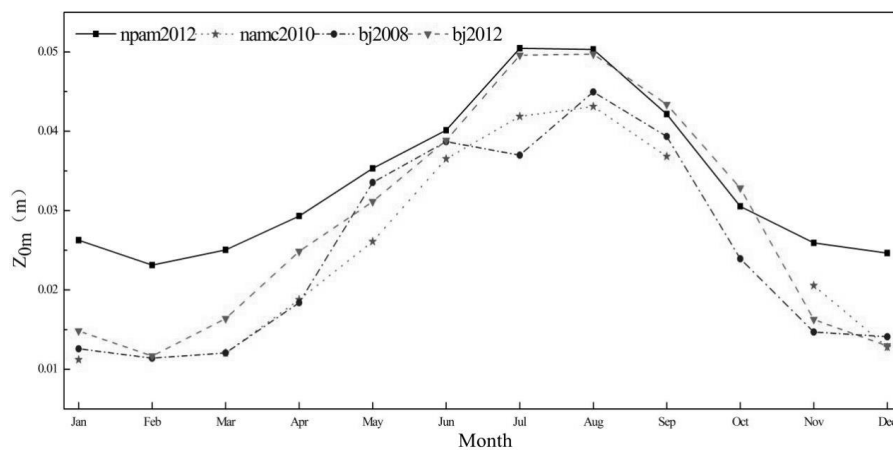


549

550 Fig. 1 The location of sites and the land cover on the northern of the Tibetan Plateau. The black

551 solid circle '●' is location of the sites.

552

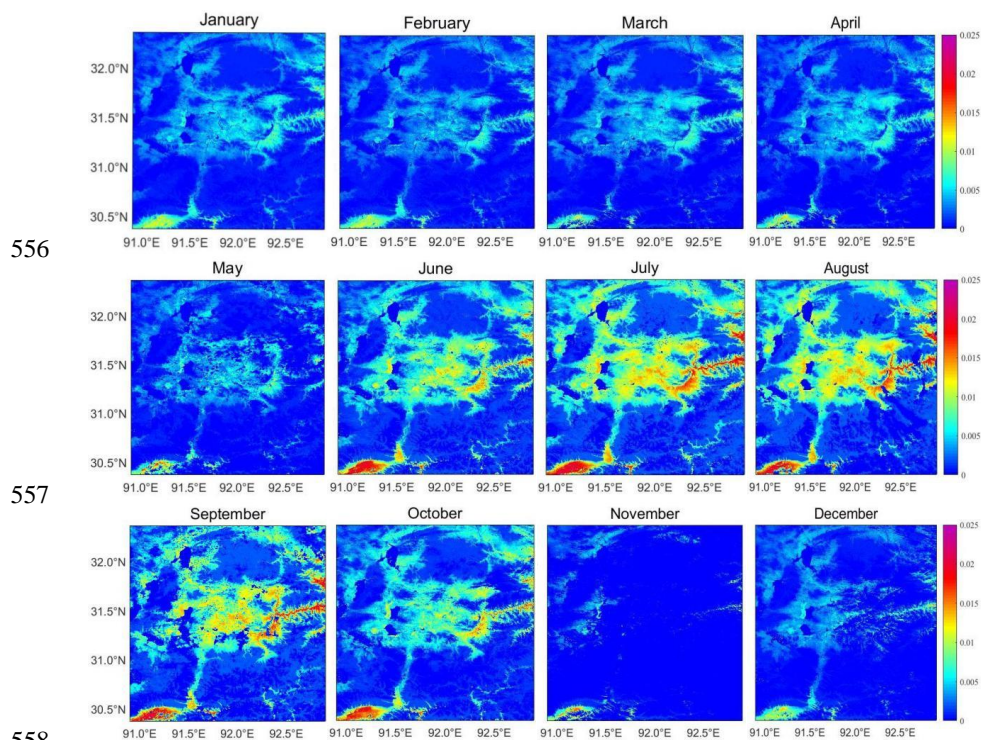


553

554 Fig. 2 The surface roughness length of different site on the northern of the Tibetan Plateau

555

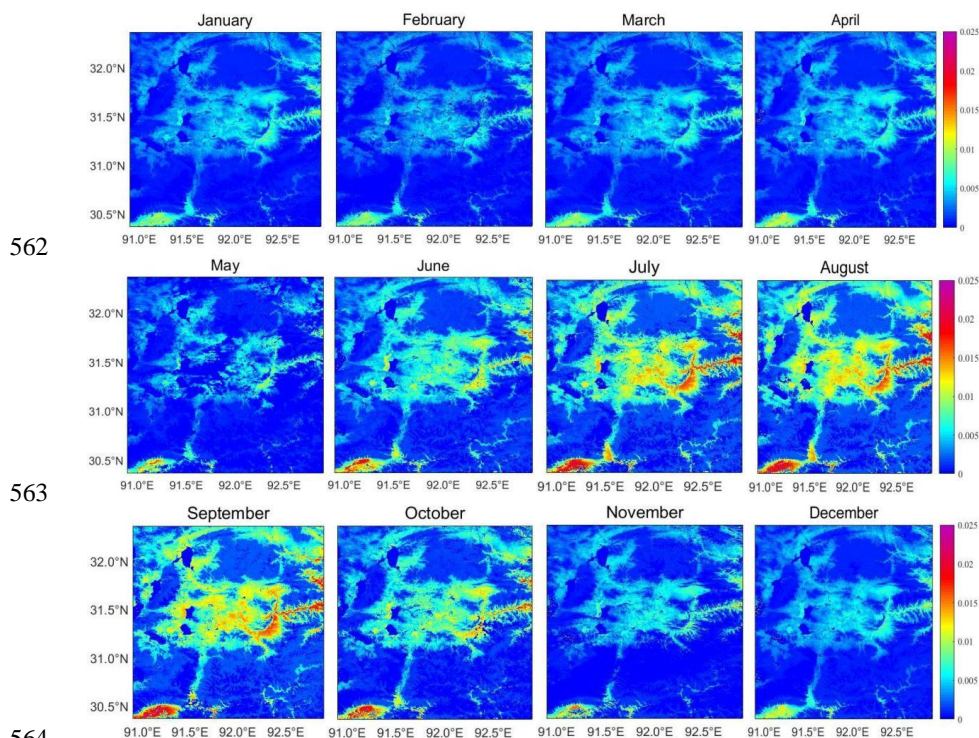




559 Fig. 3 The surface roughness length on the northern of the Tibetan Plateau in 2008

560

561



562

563

564

565

Fig. 4 The surface roughness length on the northern of the Tibetan Plateau in 2010

566

567

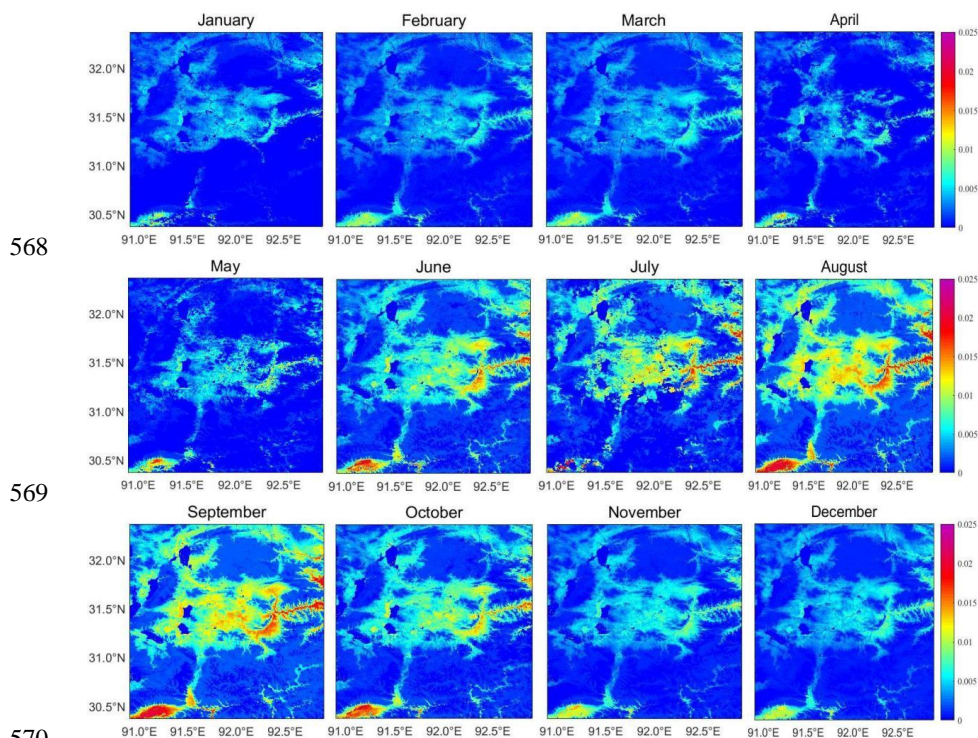
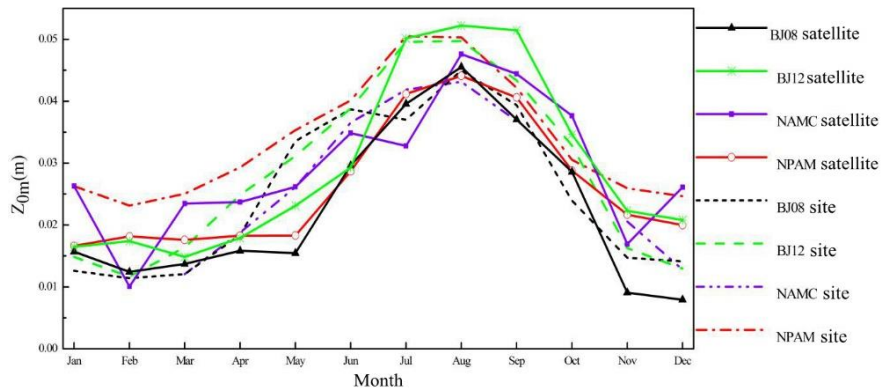


Fig. 5 The surface roughness length on the northern of the Tibetan Plateau in 2012

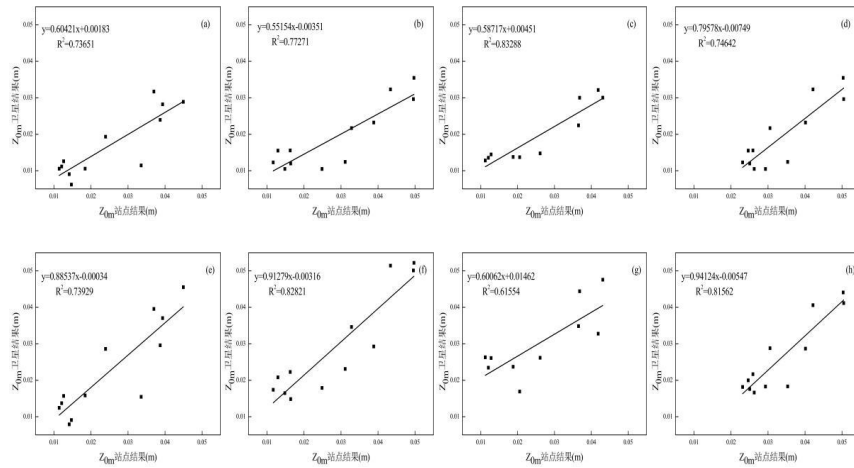


573

574 Fig. 6 Comparison of surface roughness length by site observation and satellite remote sense

575 retrieved

576



577

578

579 Fig. 7 Site surface roughness length scatter plot

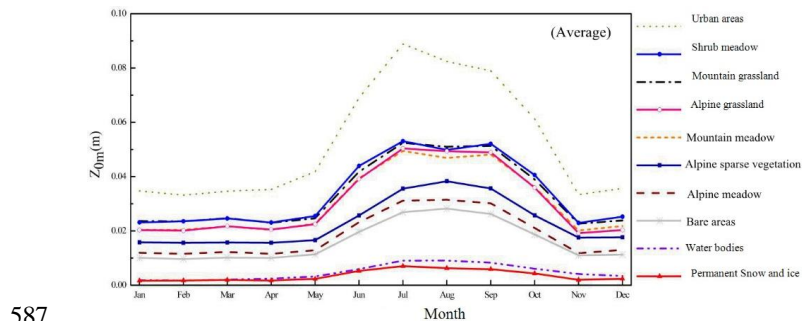
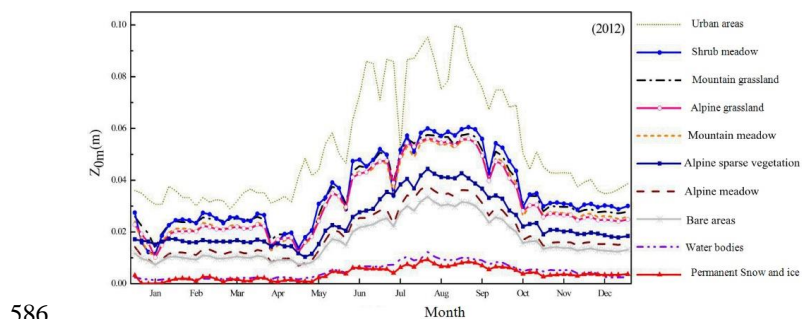
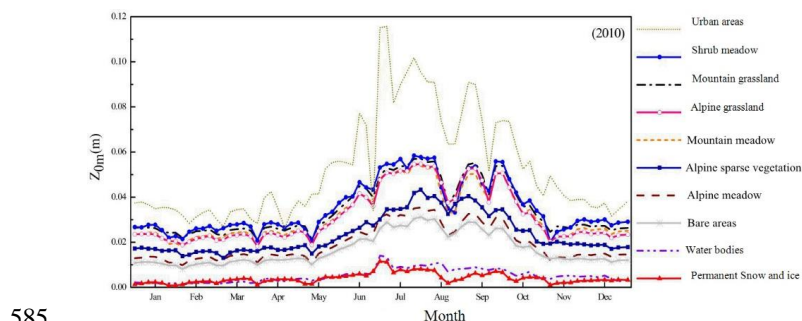
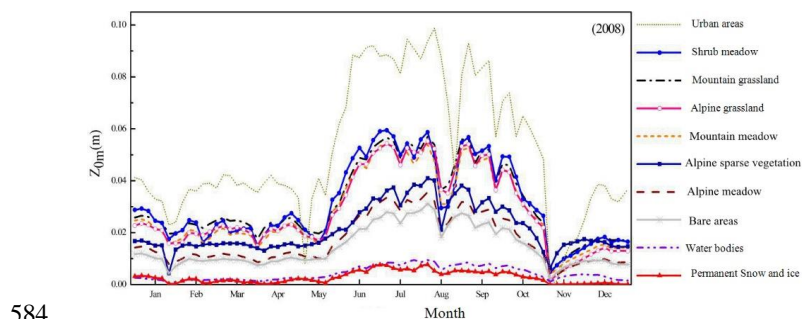
580 (a-d: scatter plot of the observation results and the average result of the underlying surface; e-h:

581 scatter plot of the observation and retrieved results; a,e: BJ station in 2008; b,f: BJ station in 2012;

582 c,g: NAMC station in 2010; d,h: NPAM station in 2012)

583





588 Fig. 8 The curve of the surface roughness length in different underlying surface

589